

# INVESTIGATING THE MICRO MECHANICS OF CEMENTED SAND USING DEM

John de Bono, Glenn McDowell, Dariusz Wanatowski

University of Nottingham, UK.

## ABSTRACT

The discrete element method has been used to investigate the micro mechanics of cemented sand. High pressure drained triaxial tests are modelled in 3D using a flexible membrane which allows the correct deformation to develop. Simulations with up to 12 MPa confining pressure are presented, which are compared with laboratory experiments on a sand with a range of cement contents. Cementation is modelled using 'parallel bonds', and various parameters and strength distributions are investigated. Varying levels of cementation are successfully modelled, with the correct qualitative behaviour observed, and the separate effects of cementation and confining pressures demonstrated. The triaxial behaviour is found to be highly influenced by the distribution of bond strengths.

## 1 INTRODUCTION

The discrete element method (DEM) has proved a useful tool for modelling granular material. DEM uses two entities: a ball and a wall to model interactions and Newton's 2<sup>nd</sup> Law together with a contact law to establish the accelerations, velocities and displacements of particles via a time-stepping scheme. The most commonly used DEM software is PFC3D [1], which is the software used by the authors to simulate cemented and uncemented sand under high-pressure triaxial conditions. As well as developing a practical method of modelling cemented sand, the purpose of this numerical study is to investigate the micro properties of cementation and their influence, and explore how these properties can reflect varying degrees of cementation across a range of confining pressures.

Cemented sand occurs naturally through a number of processes; as a result, samples exhibit a high variation in density and degree of cementation [2]. There are also difficulties involved in extracting natural specimens while avoiding disturbance. Soils may be artificially cemented to improve performance, and are commonly used in pavement subbase layers. Leroueil and Vaughan [3] used the term 'structured soils' to comprise cemented sands, over-consolidated clays, and weak rocks. They showed that these soils follow the same principal behaviour and that the physical properties of the cemented soil govern its behaviour, rather than individual causes of cementation. Hence it has been common practice to perform tests on artificially cemented sands to draw conclusions and deepen understanding [4–8].

The majority of published research on cemented sand under triaxial conditions is at conventional pressures (typically under 1 MPa). Coop and Atkinson [5] demonstrated that the addition of a cementitious material to sand introduces well defined yield points into the stress-strain response during triaxial shearing, which could be related to the breakage of cementation. At large strains, both cemented and uncemented sands reached steady conditions, i.e. critical state, and notably appeared to have the same critical state line. They outlined three modes of failure for cemented soils, defined by when yielding (breakage) of the bonding occurs. The first case is when cement

bonds break during isotropic consolidation, causing subsequent shearing behaviour similar to that of the equivalent uncemented soil. The second case is where bonds are initially intact but break during shearing, and any peak state is governed by the frictional properties of the equivalent non-structured soil. Thirdly, when the bonds yield after shearing has commenced, causing a clear peak stress to occur.

## **2 DRAINED TRIAXIAL BEHAVIOUR OF CEMENTED SAND**

### **Conventional Pressures (<1 MPa)**

At low confining pressures, Huang and Airey [9] showed that cementation causes an increase in stiffness, peak strength, maximum rate of dilation, and in general the specimen becomes more brittle (brittle behaviour is characterised by sudden failure, associated with a peak stress, followed by strain softening, and the occurrence of shear planes). These effects all increase with increasing cement content. At higher confining pressures, the cementation appears broken, and the normalised stress-strain responses for various cement contents appear identical. Schnaid et al. [10] performed a series of drained triaxial tests on cemented sand at low pressures and also demonstrated how significantly the soil behaviour is influenced by cement content. They observed an initial volumetric contraction followed immediately by a significant dilation, before a steady state was reached, with the highest cement contents exhibiting the most overall dilation. The maximum rate of dilation was found to occur just after the peak strength (dissimilar to uncemented materials—for which the maximum dilation rate coincides with peak deviatoric stress). This was due to the peak strength being controlled by the bonding rather than the initial density.

Similar behaviour has been reported by Asghari et al. [11] and Haeri et al. [12] who also categorised failure modes: brittle failure with shear planes for cemented samples and barrelling failure for equivalent uncemented samples. An increase in confining pressure suppressed the effects of cementation and caused a transition from brittle to ductile behaviour (and also increased the maximum deviatoric stress).

### **High Pressures (>1 MPa)**

Marri et al., [13] performed drained triaxial tests on sand specimens with Portland cement contents from 0–15% dry weight, across confining pressures between 1–12 MPa. In general, all uncemented specimens exhibited strain hardening with no peak deviatoric stress, and underwent contraction during shearing, demonstrating completely ductile behaviour, even with high initial densities. The addition of cement caused peak stresses to occur, and a reduction in the strain associated with this stress, and an increase in dilation. An increasing amount of cement was shown to cause the peak stress to increase and become more distinguished, and in the general caused the behaviour to become more brittle. Marri et. al. [13] also showed that with increasing cement content, the axial strain associated with the peak reduces, and the initial modulus of deformation becomes higher, and causes an increase in both the amount and rate of dilation. This is broadly consistent with previous work on artificially cemented and uncemented sands at low pressures, e.g. [14]. All of Marri's

samples had a high initial relative density, with voids ratios in the range 0.50–0.54, and typical results are given in Figure 1.

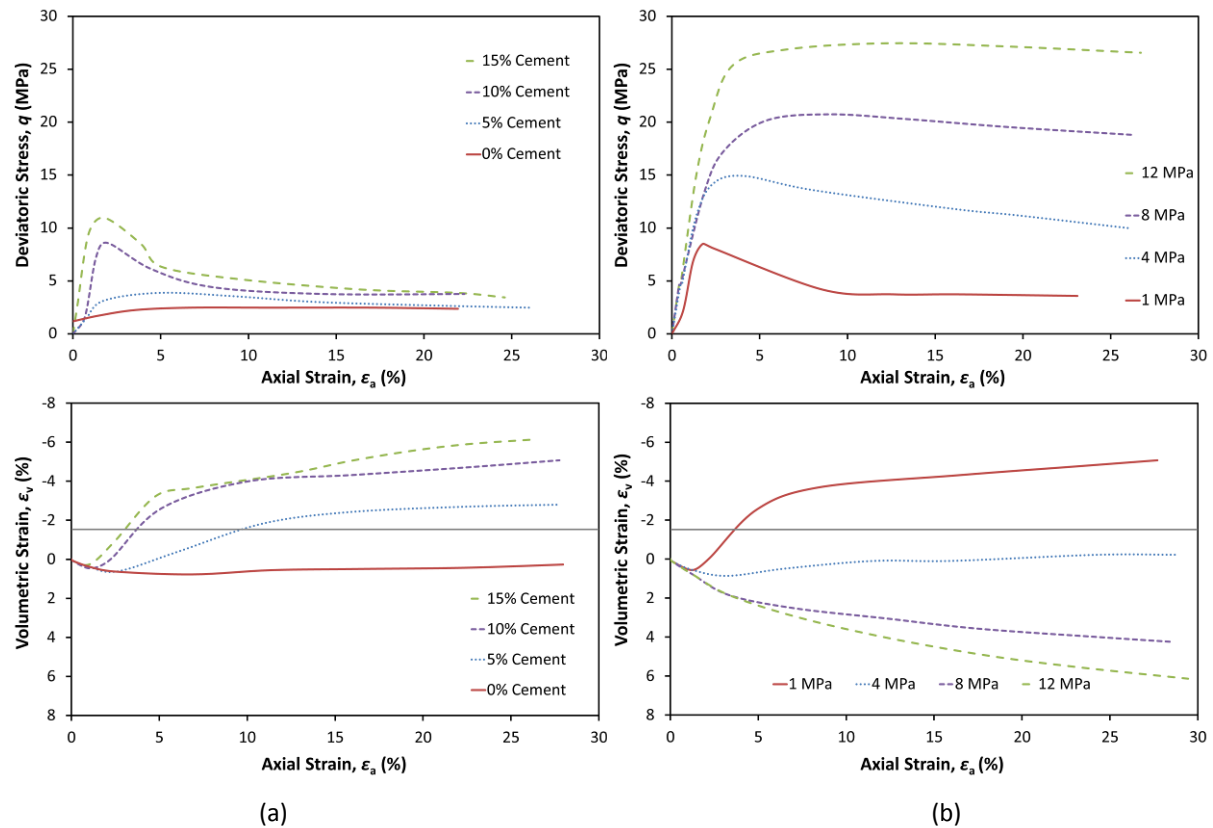


**Figure 1** Stress-strain behaviour of various cement contents under (a) 1 MPa confining pressure, and (b) 10% cement content sheared under a range of high confining pressures [13]

The effects of varying degrees of cementation are shown in Figure 1(a). For a given confining pressure, both uncemented and cemented specimens deviatoric stress responses appear to converge or be approaching convergence after large strains, due to the cemented specimens becoming ‘destructured’ and the behaviour tending towards that of the uncemented sand. However, they often do not quite converge, especially at high cement contents, due to a portion of bonds remaining intact, causing groups of particles to behave as larger particles, effectively changing the grading.

Increasing the confining pressure has equally important effects on the behaviour of cemented sand; as at conventional triaxial stress levels, this suppressed the effects of cementation, and rendered the behaviour from brittle to ductile. The cemented samples at 1 MPa demonstrate brittle behaviour, with clear peak states with strain softening, and shear planes visible in the highly cemented samples. At 12 MPa, all cemented samples demonstrated ductile failure, with gradual strain hardening and volumetric contraction, and barrelling failure modes, similar in essence to uncemented sand, although the effects of cementation were still evident. Increasing confining pressure caused higher maximum deviatoric stress, and reduced dilation. At the highest pressures, no clear peak stress is apparent, with specimens displaying ductile behaviour, with a gradually increasing deviatoric stress approaching a steady maximum value. The triaxial responses of a given cement content sheared over a range of confining pressures are shown in Figure 1(b). The specimens also underwent

contraction, in contrast to those sheared at lower pressures. However, the effects of cementation were still apparent at higher pressures when compared with the uncemented material. From lower to higher confining pressures there is a general transition from brittle to ductile behaviour. At intermediate confining pressures, such as 4 and 8 MPa, the behaviour was neither completely brittle nor ductile.

### 3 DISCRETE ELEMENT METHOD

#### Triaxial Model

A large portion of the literature currently available on modelling cemented sand using DEM has been limited to two dimensions—for example Jiang et al. [15–17], Wang & Leung [18], Uti & Nova [19], Camusso & Barla [20]. Potyondy and Cundall [21] and Schöpfer et al. [22, 23] presented three-dimensional modelling of rock, while Cheung et al. [24] presented similar work on cemented sandstone—although these works did not feature flexible boundaries, which are characteristic of laboratory triaxial tests. Wang and Tonon [25] on the other hand did use flexible boundaries when modelling rock, although the focus of their work was to highlight the advantages and importance of such boundaries, rather than the micro mechanics of inter particle bonding.

The triaxial model used here is the same as outlined in de Bono et al. [26]. This model features a flexible membrane that allows the true failure mode to develop while maintaining a constant confining pressure. The membrane consists of bonded particles a factor of ( $\frac{1}{3}$ ) smaller than the smallest specimen particle. The membrane particles are bonded by ‘contact bonds’, which are infinitesimal bonds that transmit no moments, ensuring flexibility. They are defined by normal and shear strengths, which are set high enough to avoid puncture. The confining pressure is created by applying discrete forces to the membrane particles; a full description of this model can be found in the above reference, as well as in de Bono [27].

The sample used herein has a height of 100mm and a diameter of 50mm. The sand grains are represented by spherical particles, generated using the radii expansion method [1]. The numerical sample is generated from three user-defined parameters: initial voids ratio ( $e_0$ ), coefficient of uniformity ( $C_u = d_{60} / d_{10}$ ) and the minimum sand particle diameter ( $d_{min}$ ). An identical sample is used throughout the following simulations, with the values  $e_0 = 0.55$ ,  $C_u = 2$ , and  $d_{min} = 2$  mm. The value of  $C_u = 2$  was chosen to represent Portaway Sand, used by Marri et al. [13], and is used to obtain a simplified grading curve. For a given initial voids ratio and grading, the minimum diameter  $d_{min}$  therefore directly determines how many particles are created. The particle size distribution (alongside that of Portaway Sand) is given in Figure 2. Varying the minimum particle diameter shifts the position of the grading curve, and does not necessarily change the packing geometry.

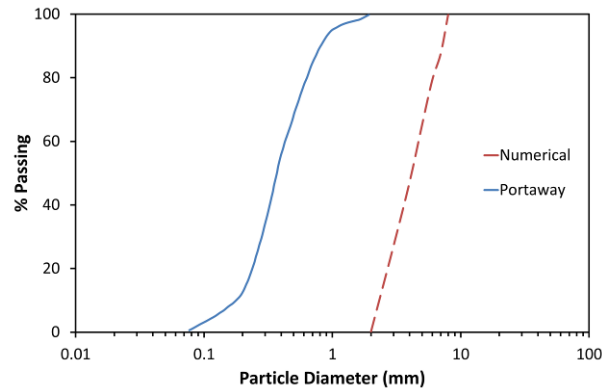


**Figure 2** Particle size distributions for the numerical specimen and Portaway sand

The initially dense specimens consist of 6759 particles each, and are confined by a membrane consisting of 11979 smaller particles. This number of sand particles cannot be considered realistic, it is however a larger amount than that used in much of the research mentioned earlier (typically less than 2500). Although some relevant DEM studies have used a noticeably larger number of particles [23, 24], these studies invariably used uniformly graded samples, usually with rigid boundaries—which prohibit the sample from deforming as it would do in a laboratory test with a flexible membrane. When simulating a wide range in particle sizes—as is the case here—the overall number of particles allowed is severely limited by the simulation time. The modelling of the membrane requires (in this case)  $\approx 12000$  particles, which is already computationally intensive, hence with a ratio of 6:1 between the largest and smallest simulation particles, a total of 6759 sample particles was deemed reasonable. Collop et al. [28] showed that for elastic simulations on bonded asphalt samples, 4500 particles appeared sufficient to give representative values of Young’s Modulus; however it should be acknowledged that due to the sample geometry, boundary effects may propagate into a sizable volume of the material and influence the results [29, 30]. Although the high-resolution flexible membrane will help to reduce this effect, the observed behaviour may not necessarily reflect the true material response, and as such this work should be considered solely a parametric study.

Wang & Leung [18] suggested using a normal particle stiffness of the order  $10 \cdot 10^6$  N/m for quartz sand, and that the same value can be used for both normal and shear stiffness. In the simulations presented here, the sand particles were given a normal stiffness of  $10 \cdot 10^6$  N/m, and to reduce the number of input parameters, the same assumption was made and shear stiffness was also assigned this value. Density was set at  $2650 \text{ kg/m}^3$ , reflecting the density of the sand used in the aforementioned laboratory experiments [13], and a particle friction value of 0.5 was attributed. Platen friction was set to zero. A summary of the sample and membrane DEM properties are given in Table 1. After confinement was applied, the top platen was accelerated gradually to 0.05 m/s; this was found to be the maximum velocity possible while ensuring that the top and bottom platen stresses remained equal to one another. The damping coefficient was left at its default value.

It should be noted that using spheres fails to reflect the irregular shape of real sand particles—realistic shape would change the mechanical behaviour of the numerical soil, however the work presented here is a necessary, fundamental step required before implementing realistic shape using ‘clumps’ of balls.

**Table 1** Summary of DEM properties of the sample and membrane

<b>Sample Properties</b>	
Size: Height x Diameter (mm)	100 x 50
No. of Particles	6759
Friction coefficient	0.5
Normal and shear stiffness (N/m)	$10 \times 10^6$
Density ( $\text{kg/m}^3$ )	2650
Coefficient of uniformity	2.0
Minimum particle diameter (mm)	2.0
Maximum particle diameter (mm)	8.0
Initial voids ratio	0.55
Contact model	Linear springs (default)
Damping coefficient	0.7 (default value)
Bond diameter (mm)	2
Mean bond normal and shear strength ( $\text{N/mm}^2$ )	15.92*
Mean equivalent bond strength in pure tension and pure shear (N)	50*
<b>Membrane Properties</b>	
No. of particles	11979
Friction coefficient	0.0
Normal and shear stiffness (N/m)	$0.6 \times 10^6$
Density	1000
Particle diameter (mm)	1.33

\*unless stated otherwise

### Inter-Particle Bonding

Cement bonds are modelling using ‘Parallel Bonds’, a feature of the software [1]. These consist of a finite-sized cylindrical piece of material between the two particles, which acts in parallel with the standard force-displacement contact model. These were developed by Potyondy & Cundall [21], and have been used in numerous previous studies, e.g. Wang & Leung [18], Schöpfer et al. [22, 23], Cheung et al. [24]. The bonds are defined by normal and shear stiffness (in terms of stress/displacement), normal and shear strength (in terms of stress) and bond size per unit area of the bond.

There are various approaches to choosing the size of the cement bonds; one might consider them as small relative to the particles, occurring just at the contacts and independent of particle size [18, 31], or alternatively to consider them as proportional to the particles, filling much of the void space [24]. Both of these approaches seem justifiable depending on interpretation of the nature of cementation and—if possible—analysis of high magnification images. In this study, in order to isolate and investigate bond strength distributions, all bonds are created with equal size (radius equal to the smallest sand particle), therefore having equal moment resistance. To reduce the number of variables, and because this study is not exclusively concerned with calibration against physical tests, parallel bond stiffnesses have been defined to give values equal to the particle stiffnesses (in terms

of force/displacement), except where mentioned; although Cheung et al. [24] did investigate the effects of varying the ratio of bond to particle stiffnesses.

Bonds are installed between particles that are in direct contact (or within *very* close proximity). For a dense arrangement of particles, with the parameters described above, this method installs approximately 5 bonds per particle, and leaves a small number (4%) of free particles with no bonds. A series of simulations have been conducted to investigate solely the bond strength properties, using a triaxial sample with approximately 17000 parallel bonds (each particle has an average of 5 neighbouring particles bonded to it).

The principal effects of the parallel bonds are evident in Figure 3 where the deviatoric stress versus axial strain responses are shown from simulations of the cemented material showing the effects of varying strength (a) and stiffness (b), along with the behaviour of the uncemented sample, all sheared under a confining pressure of 1 MPa.

In Figure 3(a), the cemented samples have completely uniform bonds, i.e. there is no strength distribution. All bonds are equal in size, stiffness and strength in each test, with only the bond strength varied across the three simulations. The three different parallel bond strengths have been defined as 7.96, 15.92 and 31.83 N/mm<sup>2</sup>, to give strengths of 25, 50 and 100 N respectively in pure shear and tension. It is immediately evident that the introduction of cement bonds with strengths 50 and 100 N cause a large peak deviatoric stress to appear and increases the maximum stress compared to the unbonded sample. The simulation with bonds of strength 25 N has a smaller peak stress, with almost all the bonds breaking soon upon commencement of shearing, after which behaviour similar to the uncemented sample is observed. The peak stress witnessed in the cemented simulations is caused by the presence of bonds, with the peak appearing to coincide with the onset of major bond breakage. All bonded samples exhibit a stiffer initial response compared to the unbounded equivalent. The cemented samples approach the stress state of the uncemented simulation as the bonds eventually become broken down, and the material becomes destructured.

Inspecting the graphs of volumetric strain versus axial strain shows that the most strongly bonded sample undergoes slightly more dilation than the other simulations. Figure 3(b) shows the effects of varying stiffness by the same magnitudes (normal and shear stiffnesses of 5, 10, and 20 x 10<sup>6</sup> N/m are used). These are less pronounced, with very similar peak values of stress and dilation. The simulation with the stiffest bonds has the (slightly) lowest peak strength, and the fewest bonds remaining after shearing. The increased stiffness causes the bonds to break earlier, and therefore fewer remain to resist deformation.

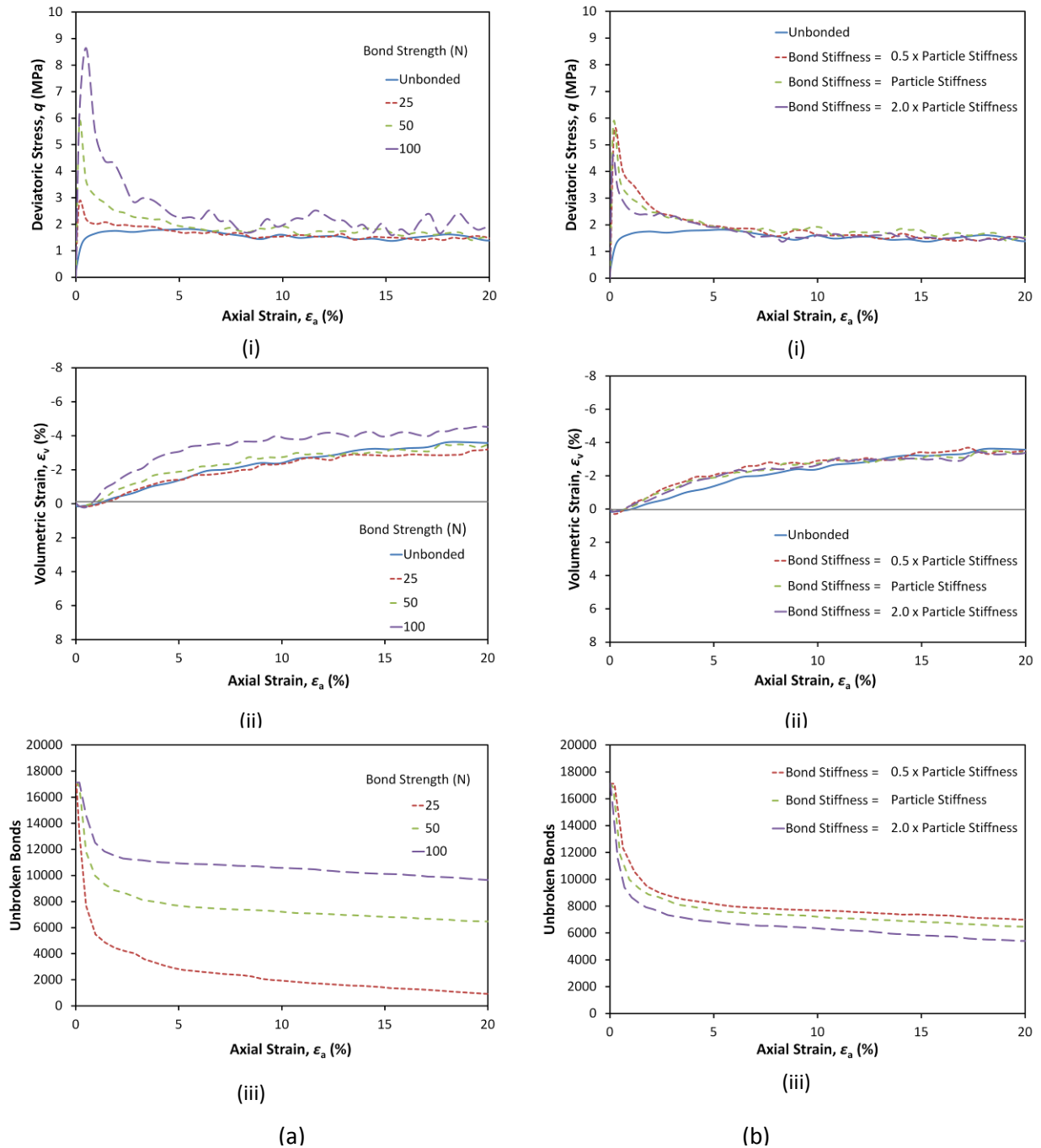


**Figure 3** Stress-strain behaviour of simulations with various bond strengths (a) and bond stiffness (b): deviatoric stress (i), volumetric strain (ii) and unbroken bonds (iii) versus axial strain

Considering again Figure 3(a), the bond uniformity is reflected in the graphs; the very sharp peak indicates extremely brittle failure and rapid onset of bond breakage. It is apparent from the graph that there is an initial linear region, during which no bonds have broken, particularly for the 100N bond strength. This seems somewhat unrealistic, especially at these stress levels. It is evident from the literature (e.g. [2,11]) that one might expect such a sharp peak with an initially linear response at very low pressures (typically  $\epsilon_a$  under 100 kPa), however, as is visible in Figure 1, no sharp peaks or such brittle behaviour is witnessed at higher pressures, with only the highest cement content

producing a *rounded* peak. One might therefore assume that a distribution of bond strengths would yield more realistic results—i.e. a more rounded peak stress with gradual bond failure. Figure 4 compares the results of cemented simulations with the same initial setup as before, but with parallel bond strengths satisfying three different probability distributions: uniform, normal and Weibull.

Figure 4(a) and Figure 4(b) show the deviatoric stress response of samples with bond strengths satisfying two alternative uniform distributions and two normal distributions, all with the same mean strength of 50 N. The bonds with uniformly distributed strengths have ranges of 50 and 100 N, and the normally distributed bonds have coefficient of variations of 0.2 and 0.4. Also included is the response of the simulation with completely uniform bonds with unique strength of 50 N, as well as the unbonded simulation.

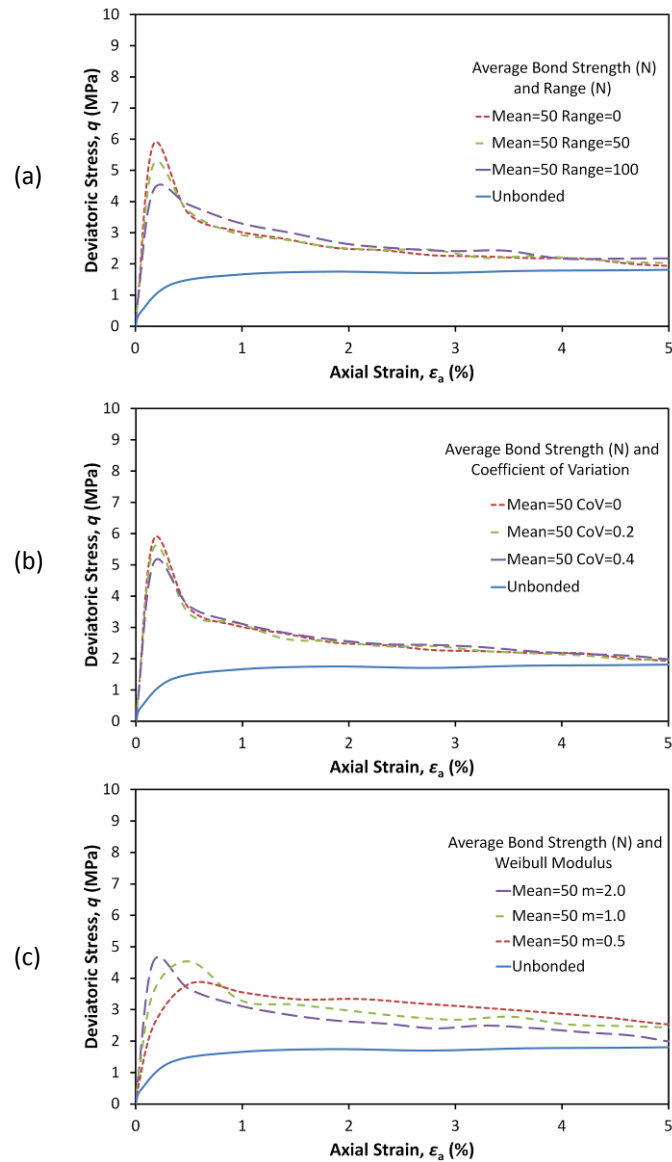
It can be seen that the samples with uniformly distributed bond strengths show lower maximum stresses, with the peaks more rounded. The sample with bond strengths ranging from 0–100 N experiences bond breakage immediately, and as such has the lowest and most rounded peak deviatoric stress. The simulation with the narrower range, i.e. bond strengths ranging from 25–75 N has a finite minimum bond strength, so there will be an initial linear region during which no bond breakage is witnessed.

The samples with normal bond strength distributions give similar stress-strain results, despite exhibiting slightly different bond breakage. The simulation with the smaller coefficient of variation behaves very similarly to the sample with no strength distribution, while the sample with the larger coefficient displays an earlier, less sudden onset of breakage. However, both the simulations with uniform and normal bond strength distributions still display sharp distinct peak stresses, indicating sudden failure due to most bond strengths lying close to the mean value. All of these simulations display approximately the same volumetric strain during shearing.

Figure 4(c) shows the results from 3 simulations with bond strengths from Weibull distributions, all with the same mean value but with differing distribution parameters. A Weibull distribution is defined by two variables, denoted in this paper as the modulus,  $m$ , and the scale parameter,  $\lambda$ . The modulus determines the shape of the distribution; the scale parameter determines the size/range. The mean of a Weibull distribution is given by:

$$\mu = \lambda \Gamma(1 + 1/m)$$

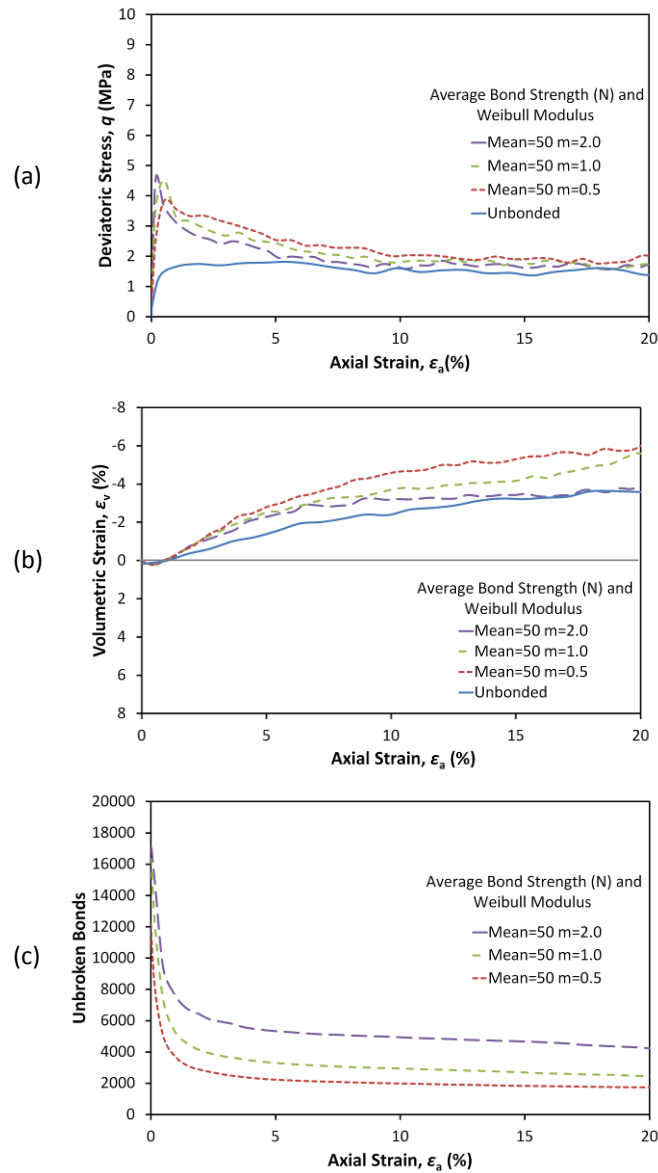
and so is affected by both parameters ( $\Gamma$  is the gamma function). Changing the modulus (shape) of a Weibull distribution slightly alters the mean, so the scale of the distribution needs to be adjusted to maintain the same mean. For a given scale,  $\lambda$ , increasing the modulus results in a narrower distribution. Weibull probability is used widely in materials science, especially in failure probability of brittle materials, so it seems reasonable that such a distribution may be applicable to cementation. It has also been used in the field of geomechanics, in particular particle breakage, for example by McDowell et al. [32, 33] and Bolton et al. [34].



**Figure 4** Deviatoric stress versus axial strain for simulations with various uniform (a), normal (b) and Weibull (c) bond strength distributions, with mean strength of 50 N

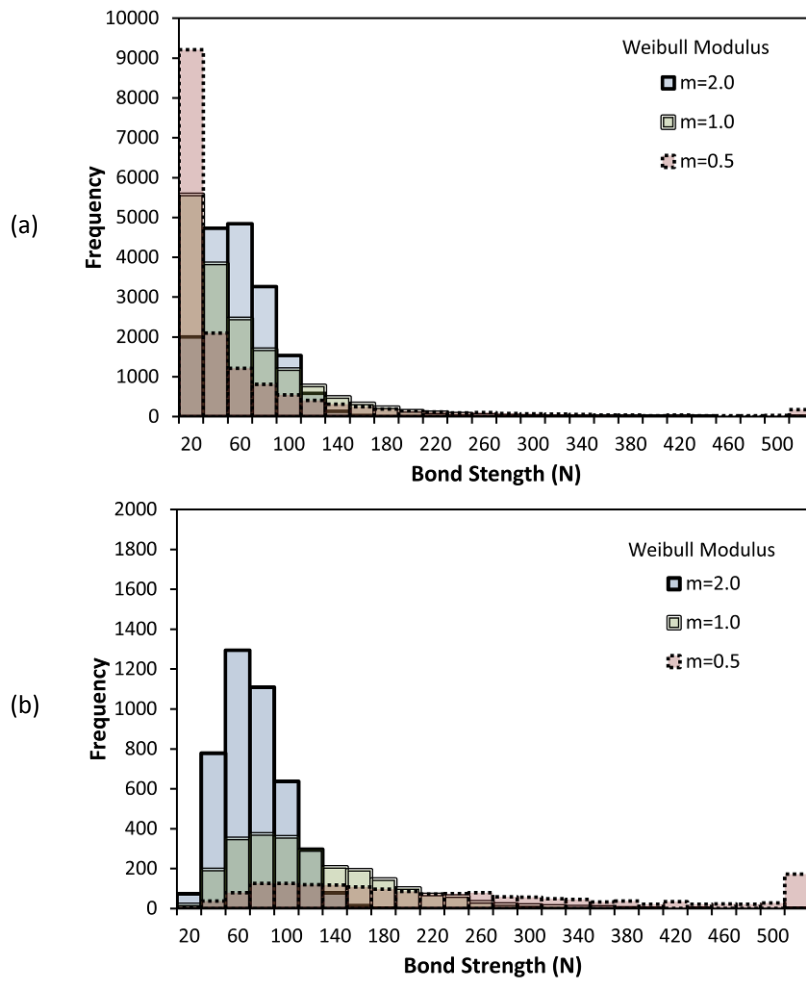
Examining the results of the various Weibull distributions of bond strengths reveals that the lower the modulus, the more rounded the peak stress. Higher values of  $m$  render the distribution and behaviour of the bonded sample similar to that with normally distributed strengths. Lower values of  $m$ , i.e. less than or equal to 1 produce a positively skewed, very wide distribution of strengths. It can be seen that the sample with a modulus of 0.5 produces a rounded peak stress, which appears the most similar to the experimental stress-stress curves at high pressures shown in Figure 1(a). This indicates a much less sudden onset of bond breakage, which is also apparent from the graph displaying the number of intact bonds versus axial strain. Although a significant number of bonds are broken during consolidation, the maximum rate of breakage during shearing is slightly lower. The full triaxial results for these simulations are shown in Figure 5, which also shows the volumetric strain versus axial strain, and the number of intact bonds versus strain. The simulation with the

lowest  $m$  value demonstrates the most dilation and also the fewest remaining bonds for a given axial strain, a different trend to that in Figure 3(a)—where the greatest dilation is associated with the *largest* number of intact bonds after shearing. This suggests that for the simulation with a Weibull modulus of 0.5, although fewest bonds remain, the bonds that *do* remain heavily influence the behaviour. For the simulation with  $m = 0.5$ , after shearing to 20% axial strain, the remaining bonds (approximately 2000) have a mean strength of 256 N covering a range of 2992 N. In contrast, the simulation with  $m = 2.0$  has approximately 4200 bonds remaining with a mean strength of 63 N covering a range of 158 N. As this is not an attempt at an exact calibration, the precise statistical model used for the bond strengths may not be of great importance. However—with the aim to improve understanding of the actual nature of bond strengths—it can be seen that a very wide, positively skewed strength distribution gives the most realistic simulation results, suggesting that this is the case for real cementation.



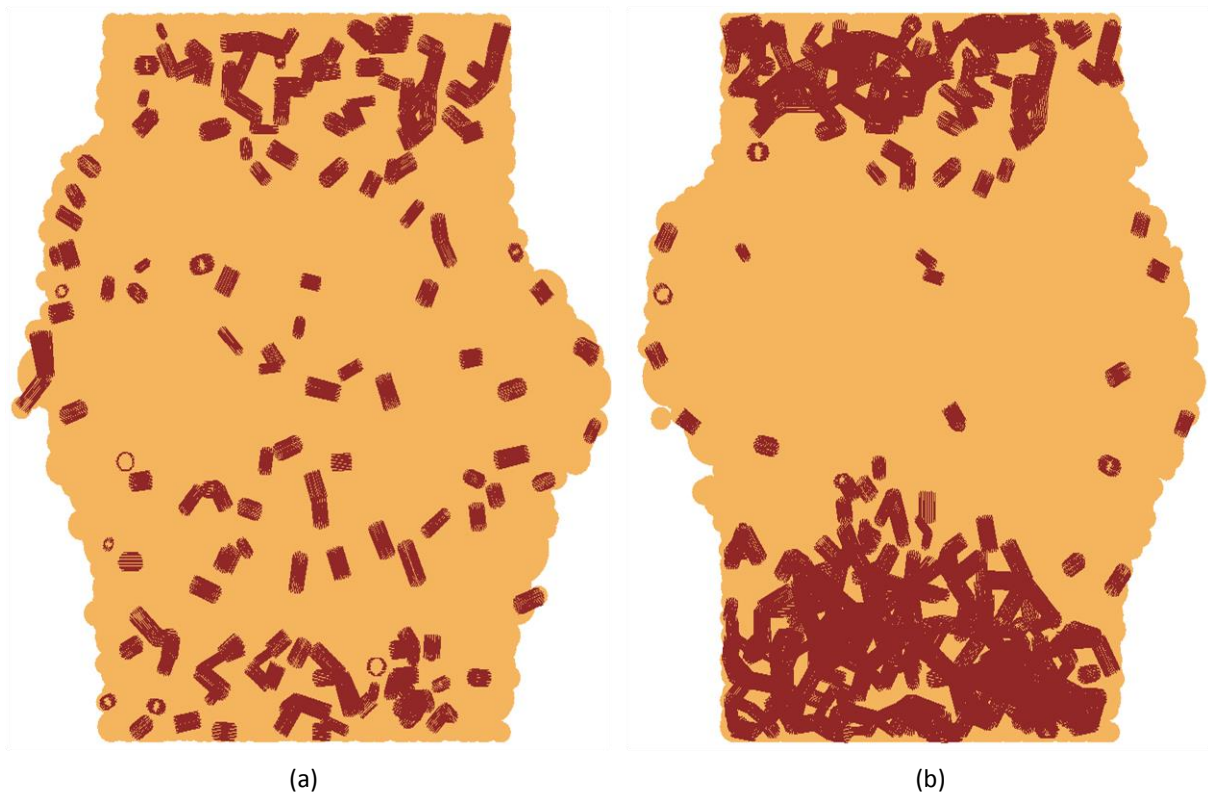
**Figure 5** Triaxial behaviour of simulations with Weibull bond strength distributions with various  $m$  values: deviatoric stress (a), volumetric strain (b) and remaining unbroken bonds (c) versus axial strain

Figure 6 shows histograms for the bond strength distributions for the three simulations with Weibull moduli 0.5, 1.0 and 2.0, before and after shearing. Figure 6(a) shows the three histograms before application of confining pressure, before any bonds have broken. Most bonds in the simulation with  $m = 0.5$  have strengths between 0–40 N, whereas in the simulation with  $m = 2.0$ , most bond strengths lie around the mean value of 50 N. Figure 6(b) shows histograms plotting the residual bond strengths after shearing to 20% axial strain, in which the difference in the quantity of remaining bonds can also be observed. While the simulation with  $m = 2.0$  (narrower distribution of strengths) has a greater number of unbroken bonds remaining, the remaining bonds in the simulation with  $m = 0.5$  are significantly stronger—there are a large number of bonds remaining with strengths over 500 N, and almost all of the weaker bonds have yielded. This suggests that it is the strengths of the *strongest* bonds that most influence the behaviour.



**Figure 6** Histograms showing the character of bond strength distributions before (a) and after (b) triaxial shearing

Inspecting the sheared samples reveals contrasting patterns of breakage; the simulation with the widest range of bond strengths ( $m = 0.5$ ) shows intact bonds distributed throughout the height of the sample, while the specimen with  $m = 2.0$  displays localised bond breakage, with most of the remaining intact bonds located close to the platens (Figure 7). During shearing, it tends to be the particles in the middle of a given specimen that will undergo the most displacement—the images suggest that for the sample with a narrow range of bond strengths ( $m = 2.0$ ), the bonds offer little resistance to this deformation, with almost no bonds remaining around the middle. For the sample with the much wider distribution ( $m = 0.5$ ), fewer total bonds remain unbroken, however there are still bonds distributed throughout the height of the sample, actively resisting shear deformation. These bonds result in ‘clusters’ of bonded particles, which effectively act as larger, irregular shaped grains, causing greater dilation when they roll over one another. This suggests that it is the strongest bonds, and their continued presence throughout shearing that controls the dilation of the material. This agrees with experimental observations mentioned earlier.

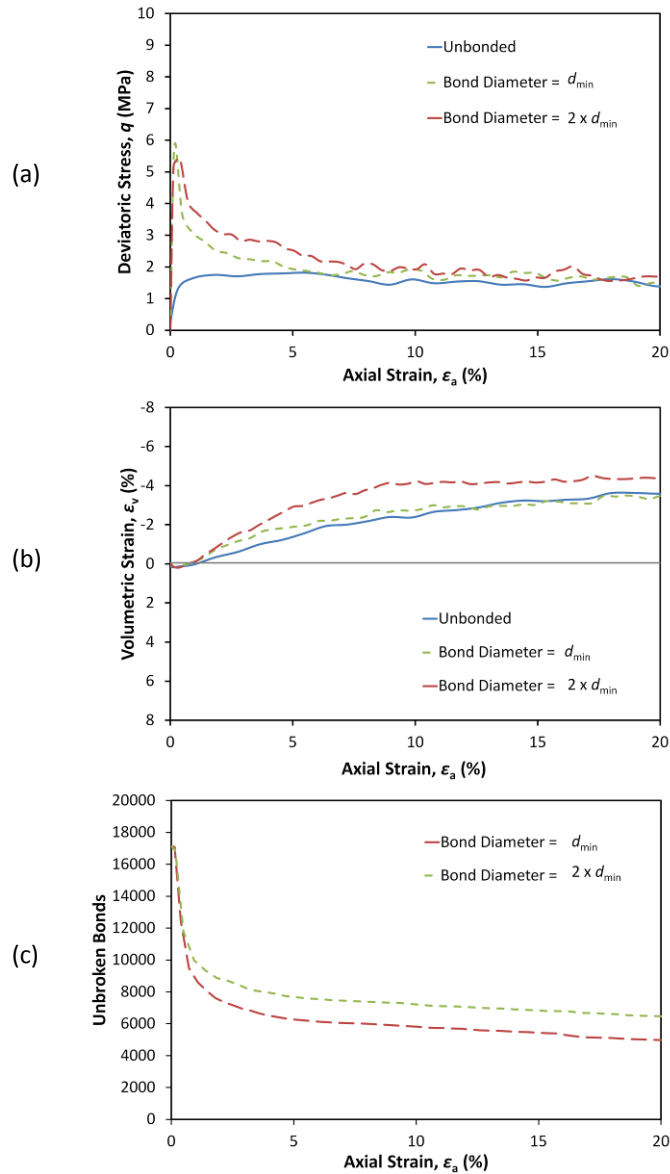


**Figure 7** Diagrams showing remaining unbroken bonds on a cross-sectional plane through the sample after 20% axial strain: sample with Weibull bond distribution with (a)  $m = 0.5$  and (b)  $m = 2.0$

### Cement Content

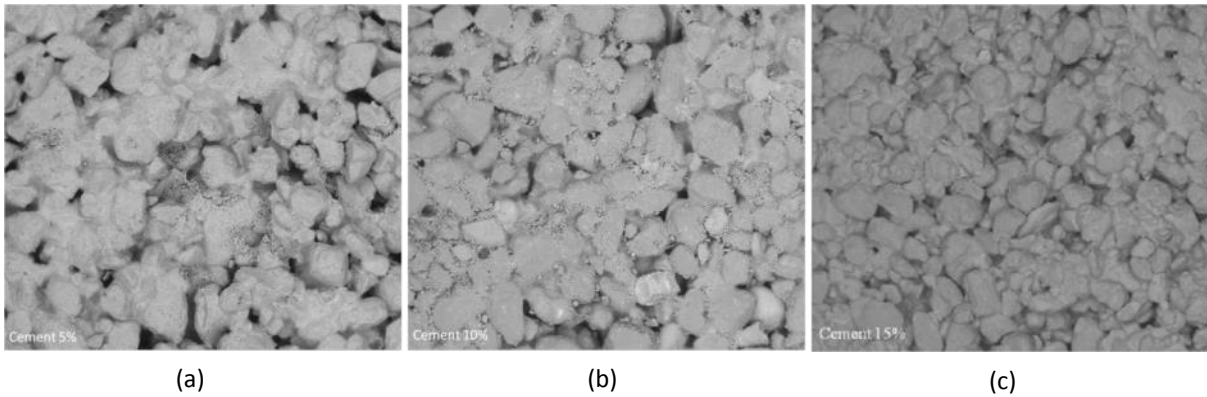
There are numerous ways in which one may consider simulating an increasing degree of cementation. Analysis of experimental data could suggest altering the variation or magnitude of bond strengths (and/or stiffness), the effects of which were shown earlier; while physical analysis may suggest altering the quantity of bonds and/or bond size.

Figure 8 highlights the effects of increasing the size of the parallel bonds. It shows the simulation from earlier where the parallel bonds have a strength of 50 N and are equal in diameter to the smallest sample particle,  $d_{\min}$ , and a simulation using parallel bonds with a strength of 50 N and diameter equal to  $(2 \times d_{\min})$ . If larger bonds are installed, the correct increase in dilation is observed, however there is very little change in the peak strength, and no effect on the specimen's initial stiffness. The increase in dilation is likely due to the increased moment resistance offered by the bonds, which hinders particles rolling over one another.



**Figure 8** Triaxial behaviour of a simulation with standard bond size (equal to the diameter of the smallest particle,  $d_{min}$ ), and a simulation with larger bond size (equal to double the diameter of the smallest particle)

Visually inspecting SEM images of the cemented sand in Figure 9 evidently suggests a greater number of bonds are required to accurately represent varying levels of cementation. The cement can be seen to fill voids and connect particles which otherwise would not be in contact. Inspecting Figure 9(a), which shows a specimen with 5% cement content, a typical sand particle visibly has 5 or 6 surrounding particles bonded to it, whereas a sand particle in the specimen with 15% cement content appears to have typically more—as many as 9 bonded to it which are visible. Bearing in the mind the planar nature of the images, one could expect a particle not on the surface of a cemented specimen to have an even greater number of surrounding particles bonded to it. Although it is admittedly not really possible to obtain a quantitative link between cement content and bonds from these images—it is however apparent that increasing the cement content results in a larger quantity of bonds between particles.



**Figure 9** Images of triaxial specimens prepared with various cement contents: (a) 5% ; (b): 10% ; (c) 15% [13]

It appears common practise when modelling bonded granular materials to install bonds at existing inter-particle contacts. For the dense numerical sample described and used above, this resulted in each particle having an average of 5 parallel bonds. Considering the proportionality between cement content and the number of bonds—indicated by Figure 9—these simulations with an average of 5 bonds per particle may be considered analogous to a given cement content. To investigate whether simply increasing the number of installed bonds is representative of increasing the cement content, a series of triaxial simulations have been performed with an increasing number of bonds. This is achieved by bonding particles which aren't necessarily touching, but which lie within a specified proximity of one another; increasing this proximity results in a larger number of bonds amongst the sand particles. Considering the quantity of bonds (in this case measured by the average number of bonds per sand particle) as a gauge of cement content, results are presented in Figure 10 for simulations with an average of 5, 10 and 20 parallel bonds per sand particle, alongside an unbonded simulation.

These quantities of bonds are somewhat arbitrary (i.e., they are not quantitatively obtained from Figure 9), and are chosen purely to demonstrate and investigate the effect of increasing the quantity of bonds. In particular, the simulation with an average of 20 bonds per particle should not be interpreted as simply artificially increasing the coordination number; it is intended to investigate the proposition that increasing cement content fills the voids, 'bridges gaps' and bonds otherwise un-touching particles. For this most heavily bonded sample, the *maximum* possible length of any parallel bond was 2 mm (theoretically the smallest particle size), which was considered the limit; increasing the bonding distance beyond this would result in numerous particles being 'intercepted' by the bonds. The simulations use the bond parameters which gave the most realistic stress behaviour (i.e. Weibull strength distribution with  $m = 0.5$  and mean strength 50 N), and all simulations are sheared under a confining pressure of 1 MPa.

From Figure 10, it can be seen that the correct qualitative behaviour with regards to modelling increased cement content is reproduced by increasing the number of bonds. There is an increase in the peak and maximum deviatoric stress, a higher initial stiffness, and there is a more dilative volumetric response. The peak stress appears at approximately the same axial strain regardless of the number of bonds. The stress-strain responses appear to converge at large strains, demonstrating good qualitative agreement with the results in Figure 1(a).

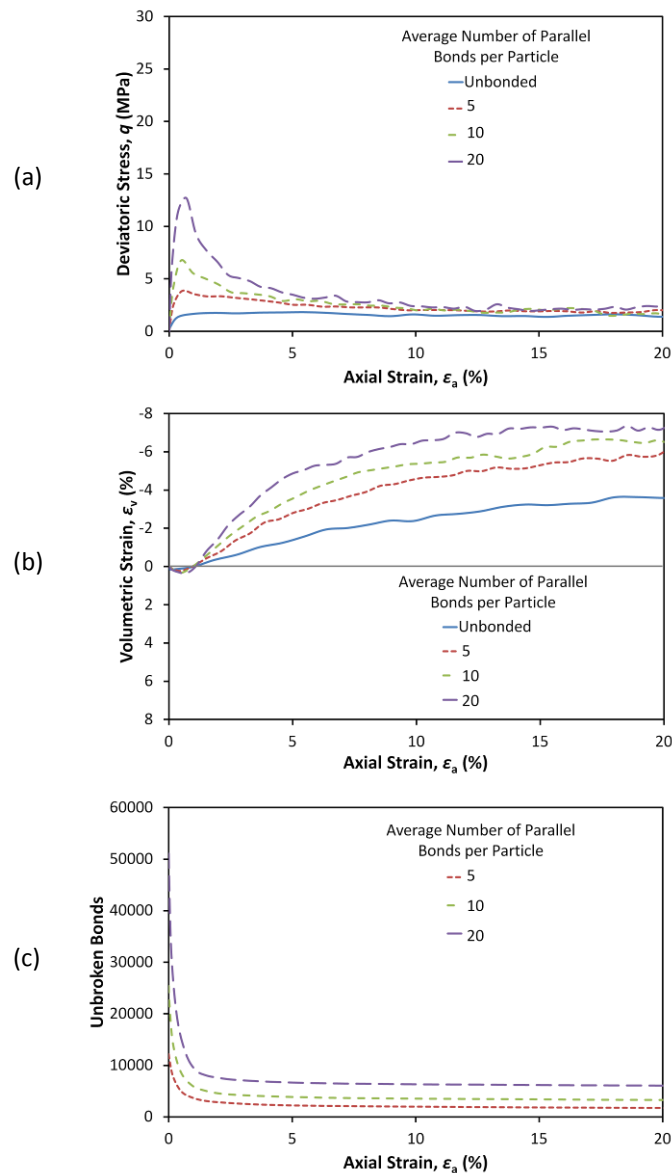


**Figure 10** Triaxial results for simulations with various number of bonds representing increasing cement content: deviatoric stress (a), volumetric strain (b) and remaining unbroken bonds (c) versus axial strain

It has been shown experimentally in the literature [35, 36] that the presence of cohesion inhibits dilatancy, and the same observation can be made in Figure 11(a), which shows the stress-dilatancy curves for the simulations with a range of cement contents. It can be seen that prior to the peak stress ratios, the most highly cemented sample (with 20 parallel bonds per particle) exhibits less dilatancy than the samples with lesser degrees of cementation, suggesting that the cohesion arising

from the parallel bonds inhibits dilatancy. This is in agreement with Cuccovillo and Coop [35], who theorised that if work is spent on degrading the bonding, which is evident from Figure 10(c), the rate of dilation has to decrease, with the bonds preventing the intact material from dilating. Prior to the peak stress ratio, Yu et al. [36] also proposed that cohesion shifts the dilatancy curve to the left when plotted in  $\eta$ - $D$  space. As in experimental findings, this ‘delay’ in dilatancy is compensated for by a rapid increase culminating in the peak dilatancy, which was largest for the most highly cemented simulation. Marri et al. [13] showed that for a given confining pressure, increasing the degree of cementation shifts the dilatancy curve upwards, resulting in larger stress ratios at the peak and ultimate states. Experimental results are repeated in Figure 11(b) for comparison. The same pattern can be observed from the simulations, although there is not a considerable difference between the ultimate states.

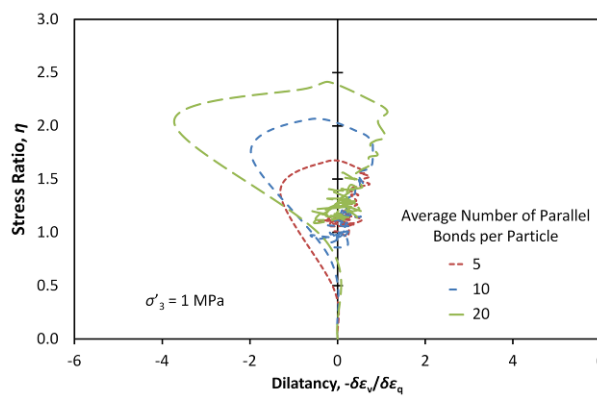


**Figure 11** Stress–dilatancy curves from simulations showing the effect of increasing the degree of cementation

### Confining Pressures

Using the bond parameters which give the most realistic stress-strain behaviour (i.e. Weibull distribution with  $m = 0.5$  and mean strength 50 N) triaxial simulations have been performed over a range of high confining pressures (1–12 MPa) and various cement contents. Assuming that the average number of bonds per particle is representative of a given cement content, Figure 12 shows the effects increasing the confining pressure has on the behaviour of cemented sand. The behaviour of samples with an average of 0, 5, 10 and 20 bonds per particle (considered uncemented, and lightly, moderately, and highly cemented respectively) are plotted for confining pressures of 1, 4, 8 and 12 MPa.

From the graphs in Figure 12, it is clear that increasing the confining pressure leads to a higher maximum deviatoric stress. The strain associated with the maximum deviatoric stress increases with confining pressure. The simulation with the medium cement content in Figure 12(c) is comparable with the experimental results shown earlier in Figure 1(b)—the strain associated with the maximum deviatoric stress increases with confining pressure, and the peak is much more prominent at lower pressures, becoming less distinguished at 12 MPa. As with experimental results, there is a transition from brittle to ductile behaviour, with the effects of cementation/bonds being suppressed by increasing confinement.

Confining pressure also greatly reduces the volumetric dilation, with the samples becoming more contractive with increased confining pressure. It can be seen that the axial strain associated with the maximum rate of dilation increases with increasing confining pressure, in the same manner as the experimental results shown in Figure 1(b). However, the correct magnitude of contraction is impossible to attain in the simulations without taking particle crushing into consideration. This also is the reason why there exists a peak in the deviatoric stress graphs, even at pressures as high as 12 MPa.

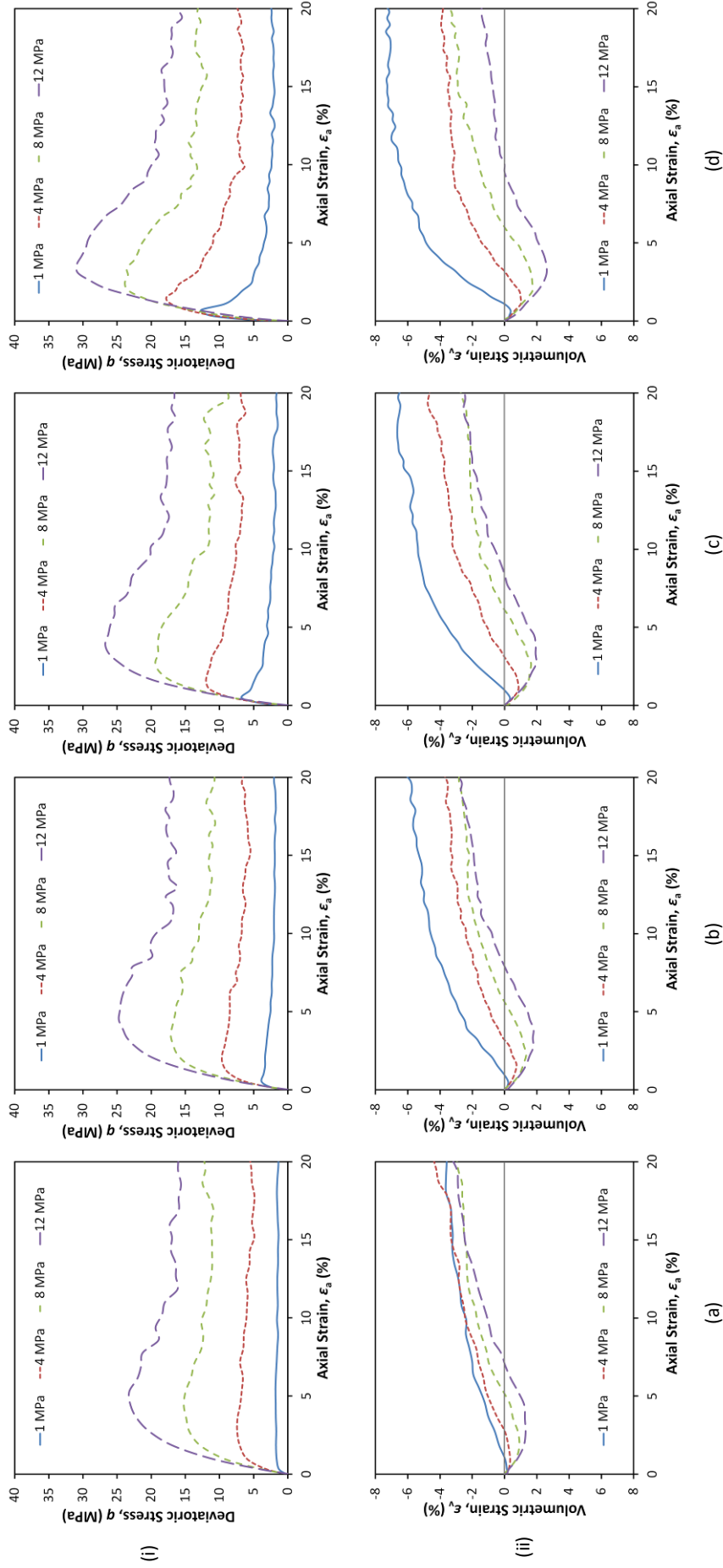


**Figure 12** Triaxial Behaviour of unbonded sample (a), and samples with an average of 5 (b), 10 (c) and 20 (d) parallel bonds per particle, sheared across a range of high confining pressures (1–12 MPa): deviatoric stress (i) and volumetric strain (ii) versus axial strain.

The dilatancy plots for the moderately cemented simulations with confining pressures 1–12 MPa are given in Figure 13(a). Increasing confining pressure reduces the peak dilatancy, as well as reducing peak stress ratio. Increasing the confining pressure generally shifts the dilatancy curve downwards in  $\eta$ - $D$  space, which offers good agreement with the experimental work by Yu et al. [36] and Marri et al. [13], the latter of which is repeated below in Figure 13(b).

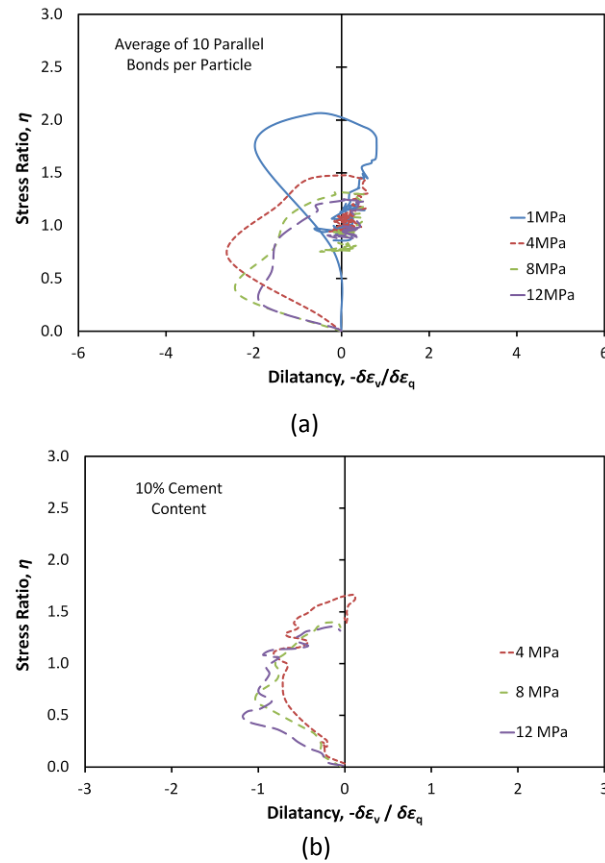


**Figure 13** Stress–dilatancy curves from simulations (a) showing the effect of increasing the confining pressure, compared with experimental results (b) [13]

### Failure Characteristics

The peak failure data from the triaxial simulations for all cement contents are plotted in Figure 14. The envelopes are obtained by fitting linear trend-lines to the failure points from simulations across the full range of confining pressures. While it is not accurately possible to observe if the failure envelopes are curved as seen in some experimental studies (e.g.[11]), it can be seen that increasing the cement content moves the failure envelopes upwards to higher stress levels in  $q$ - $p'$  space, as one would expect. The failure envelopes also show that the failure stress increases with confining pressure. The inclination of the envelopes appears to decrease slightly with increasing cement content, suggesting convergence towards very high pressures, as alluded to in the literature [13, 35, 37]. This observation indicates that the strength from cementation reduces when under high mean effective stresses, as bonds are broken during confinement. Therefore the influence of cement is greatest at lower pressures, as stated by authors such as Asghari et al. [11]. The envelopes are extrapolated, which give increasing failure stresses at zero confinement with increasing cement

content, supporting the idea that increasing the cement content (i.e. the number of inter-particle bonds) increases the cohesion.

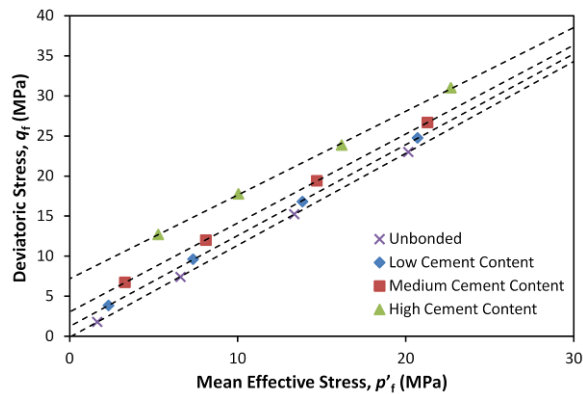
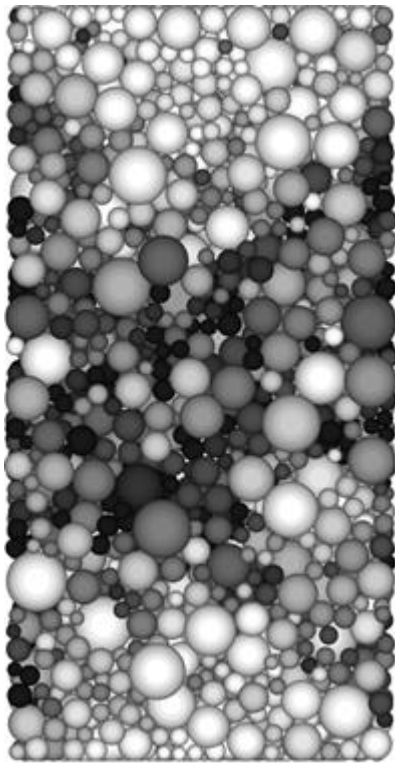
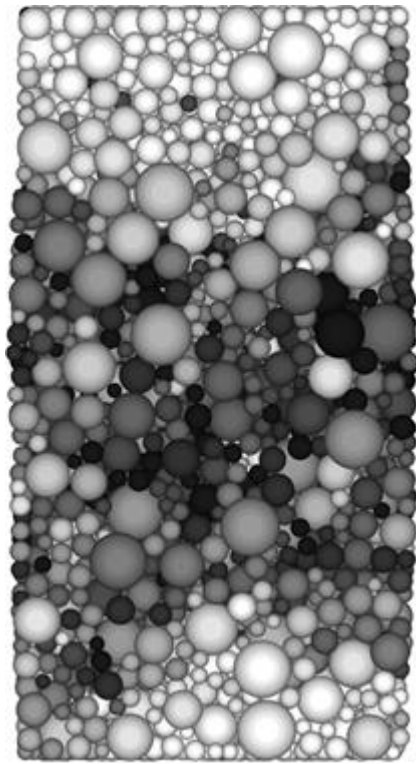


**Figure 14** Failure envelopes of simulations with various cement contents

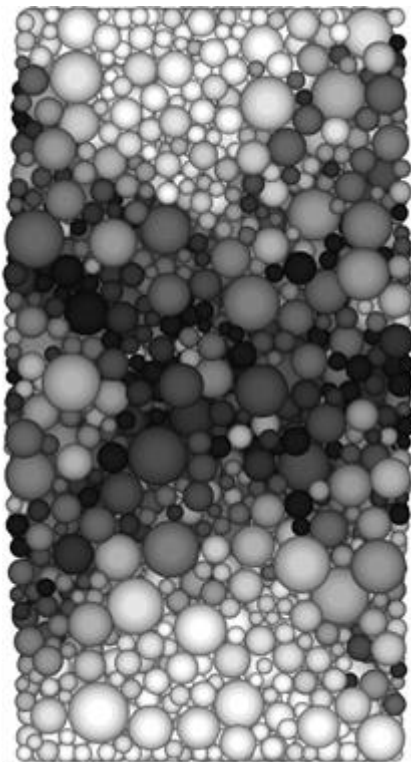
Increasing the number of bonds for a given confining pressure produces the correct transition from ductile to brittle failure. The difference in failure modes is most visible in Figure 15 which displays the particle rotations at approximately the point of maximum rate of dilation (2–3% axial strain) for simulations with various cement contents sheared at 1 MPa. The unbonded and lightly cemented samples display no clear patterns, and exhibit classic barrelling failure, while the moderately cemented sample (10 bonds per particle) displays a pair of shear bands, and the most heavily cemented sample displays a prominent steep shear plane, typical of a highly cemented, brittle material. The transition is in agreement with the literature (e.g. [10, 11]). Also visible from (c) and (d) is the indication that increasing cementation increases the inclination of the shear band, as suggested by Haeri et al. [12].



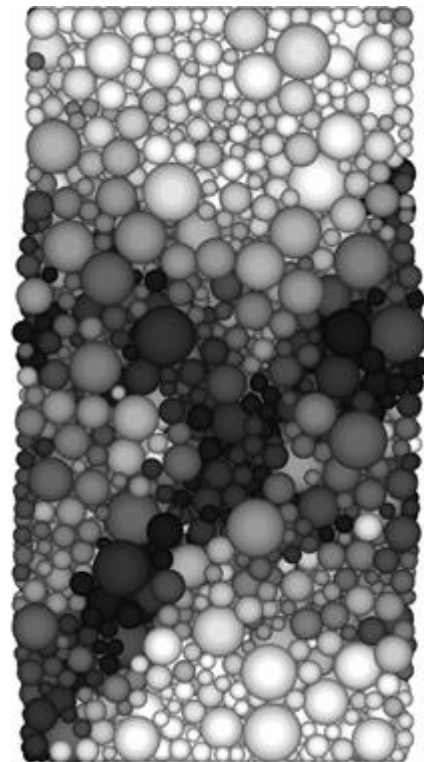
(a)



(b)



(c)



(d)

**Figure 15** Images displaying particle rotation for samples sheared under 1 MPa confining pressure at maximum rate of dilation: unbonded sample (a), lightly cemented (b), moderately cemented (c) and heavily cemented sample (b). Dark greyscale indicates particles which have undergone the most rotation; white denotes the least.

The change in failure behaviour resulting from increasing the confining pressure (from brittle to ductile) is also visible in the sheared samples: Figure 16 plots the particle rotations at approximately the maximum rate of dilation (approximately 2–6% axial strain) for the moderately cemented simulations sheared under 1, 4, 8 and 12 MPa confining pressures. Conjugate shear bands are visible in the simulation at 1 MPa confining pressure, with shear zones barely visible in the 4 MPa simulation, and no distinct patterns visible at 8 or 12 MPa. Figure 17 shows the final numerical specimens (again with moderate cement content) from the 1 and 12 MPa simulations after 20% axial strain, alongside the equivalent laboratory samples from Marri et al. [13]. From the images of the laboratory specimens after shearing, conjugate shear planes can be observed through the membrane for the sample with 10% cement content sheared at 1 MPa. Similar failure can be seen in the corresponding image of the numerical sample, which has fairly distinctive non-uniform deformations. The same material shearing under a confining pressure of 12 MPa displays barrelling failure, i.e. expansion which is uniform in the radial direction, and concentrated around the mid height of the specimen.

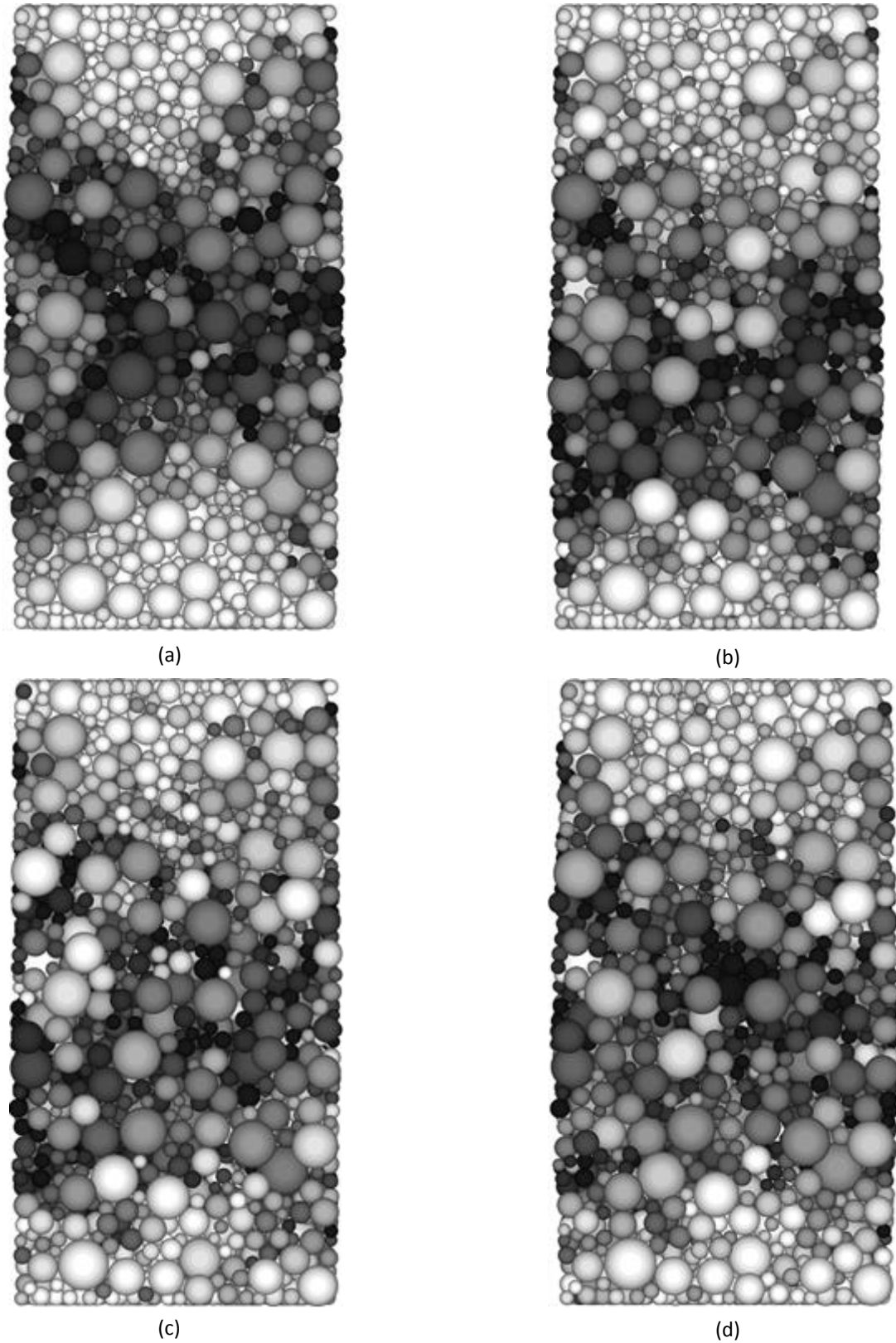


**Figure 16** Images displaying particle rotation for moderately cemented samples at maximum rate of dilation (2–6% axial strain): 1 MPa (a), 4 MPa (b), 8 MPa (c) and 12 MPa confining pressure (d). Dark greyscale indicates particles which have undergone the most rotation; white denotes the least.

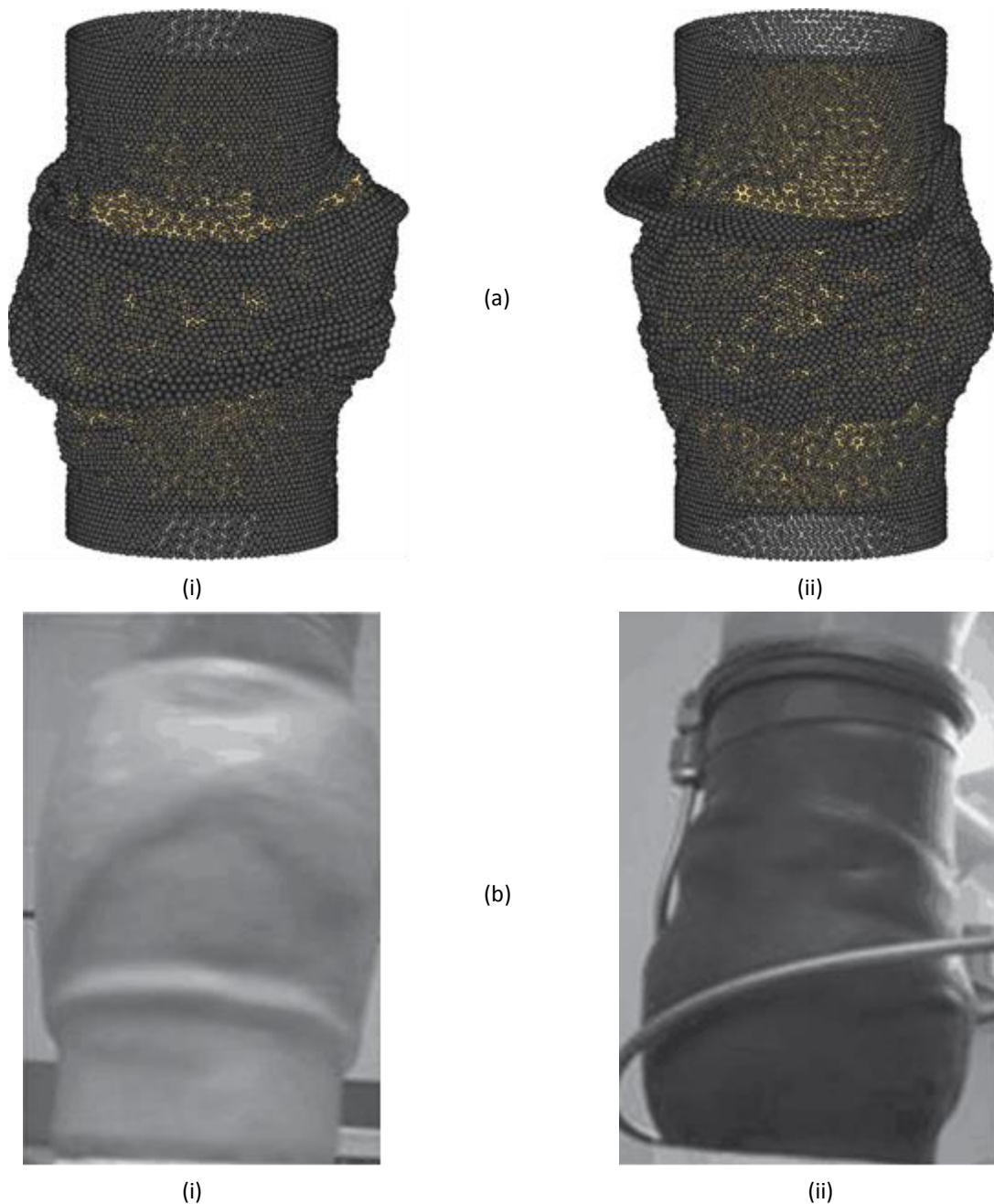


**Figure 17** Cemented numerical sample (a) and laboratory sample (b; [13]) after shearing to 20% axial strain under 1 MPa (i) and 12 MPa (ii) confining pressures

#### 4 CONCLUSIONS

A series of DEM simulations of high pressure triaxial tests have been performed on cemented and uncemented materials. The cementation has been modelled with parallel bonds, and a variety of bond strength distributions have been investigated. For a given mean bond strength, a Weibull distribution with a modulus of 0.5 appears to give the most realistic results; with some bonds failing during consolidation and immediately after commencing shearing, while the strongest remain intact throughout the tests. Such a distribution produces a sharp peak strength at lower confining pressures, and a more rounded peak at the highest pressures. The presence of bonds, which

represent cementation, also cause additional dilation when compared to the uncemented simulations. For a sample with a given number of bonds and initial density, the results indicate that it is the strength of the strongest bonds which govern any additional dilation caused by cementation.

Increasing the quantity of bonds in a given sample appears to be the most effective way of modelling increased cemented content. For a distribution of bond strengths, increasing the quantity, by bonding particles to neighbouring ones which aren't in contact but lie within a specified proximity, results in the correct qualitative change in behaviour that an increase in cement content causes in laboratory triaxial tests. It causes a more clearly defined peak strength, an increase in strength/maximum deviatoric stress, increases the dilation, and renders the behaviour more brittle.

The flexible membrane used in this study has allowed the correct failure modes to develop, allowing contrasting brittle and ductile failure modes caused by varying the cement content. By plotting the individual particle rotations, it has been shown that for a given confining pressure such as 1MPa, increasing the number of bonds (i.e. the degree of cementation) increases the strength and brittleness of the material, with shear planes produced in the most highly cemented simulations. For a given cement content, increasing the confining pressure to 12MPa suppresses the behaviour of the cementation, with no shear planes visible for even the most highly cemented samples. In between these pressures there is 'transitional' behaviour where the material behaves neither completely brittle nor ductile. DEM has therefore been shown to be able to capture the behaviour of cemented sand under a range of confining pressures and cement contents.

Work that incorporates particle crushing in this triaxial model is ongoing, and aims to enable much more realistic and insightful simulations of high-pressure triaxial tests to be performed. Future work will also aim to use a much larger number of specimen particles, as the number used in this study was unrealistic compared to laboratory samples.

## 5 REFERENCES

1. Itasca: *Theory and Background, PFC-3D Version 3.1*. Itasca Consulting Group, Inc.: Minneapolis, 2005.
2. Airey, D. W., Triaxial testing of naturally cemented carbonate soil, *Journal of Geotechnical Engineering*, **1993**; **119(9)**, pp. 1379-1398.
3. Leroueil, S., Vaughan, P., The general and congruent effects of structure in natural soils and weak rocks. *Geotechnique*, **1990**; **40(3)**, pp. 467-488.
4. Clough, G., Sitar, N., Bachus, R., Rad, N., Cemented Sands under Static Loading, *Journal of Geotechnical Engineering*, **1981**; **107**, pp. 799-818.
5. Coop, M. R., Atkinson, J. H., The mechanics of cemented carbonate sands, *Geotechnique*, **1993**, **43(1)**, pp. 53-67.
6. Haeri, S. M., Hamidi, A., Tabatabaee, N., The effect of gypsum cementation on the mechanical behavior of gravely sands, *Geotechnical Testing Journal*, **2005**, **28(4)**, pp. 380-390.
7. Alvarado, G., Lui, N., Coop, M. R., Effect of fabric on the behaviour of reservoir sandstones, *Canadian Geotechnical Journal*, **2012**, **49(9)**, pp 1036-1051.
8. Rios, S., da Fonseca, A. V., Baudet, B. A., On the shearing behaviour of an artificially cemented soil, *Acta Geotechnica*, **2013**, **9(2)**, pp 215-226.
9. Huang, J. T., Airey, D. W., Properties of artificially cemented carbonate sand, *Journal of Geotechnical and Geoenvironmental Engineering*, **1998**, **124(6)**, pp. 492-499.
10. Schnaid, F., Prietto, P., Consoli, N., Characterization of Cemented Sand in Triaxial Compression, *Journal of Geotechnical and Geoenvironmental Engineering* **2001**, **127(10)**, pp. 857-868.
11. Asghari, E., Toll, D., Haeri, S., Triaxial behaviour of a cemented gravelly sand, Tehran alluvium, *Geotechnical and Geological Engineering* **2003**, **21(1)**, pp. 1-28.
12. Haeri, S. M., Hosseini, S. M., Toll, D. G., Yasrebi, S. S., The behaviour of an artificially cemented sandy gravel, *Geotechnical and Geological Engineering*, **2005**, **23(5)**, pp. 537-560.
13. Marri, A., Wanatowski, D., Yu, H. S., Drained behaviour of cemented sand in high pressure triaxial compression tests, *Geomechanics and Geoengineering*, **2012**, **7(3)**, pp. 159-174.
14. Abdulla, A. A., Kioussis, P. D., Behavior of cemented sands-I. Testing, *International Journal for Numerical and Analytical Methods in Geomechanics*, **1997**, **21(8)**, pp. 533-547.
15. Jiang, M., Leroueil, S., Konrad, J.-M., Yielding of microstructured geomaterial by DEM analysis, *Journal of Engineering Mechanics*, **2005**, **131(11)**, pp. 1209-1213.
16. Jiang, M., Yu, H.-S., Leroueil, S., A simple and efficient approach to capturing bonding effect in microstructured sands by discrete element method, *International Journal for Numerical Methods in Engineering*, **2007**, **69(6)**, pp. 1158-1193.
17. Jiang, M. J., Yan, H. B., Zhu, H. H., Utili, S., Modeling shear behavior and strain localization in cemented sands by two-dimensional distinct element method analyses, *Computers and Geotechnics*, **2011**, **38(1)**, pp. 14-29.
18. Wang, Y., Leung, S., A particulate-scale investigation of cemented sand behavior, *Canadian Geotechnical Journal*, **2008**, **45(1)**, pp. 29-44.
19. Utili, S., Nova, R., DEM analysis of bonded granular geomaterials, *International Journal for Numerical and Analytical Methods in Geomechanics*, **2008**, **32(17)**, pp. 1997-2031.
20. Camusso, M., Barla, M., Microparameters calibration for loose and cemented soil when using particle methods, *International Journal of Geomechanics*, **2009**, **9(5)**, pp. 217-229.

21. Potyondy, D. O., Cundall, P. A., A bonded-particle model for rock, *International journal of rock mechanics and mining sciences*, **2004**, **41(8)**, pp. 1329-1364.
22. Schöpfer, M. P. J., Abe, S., Childs, C., Walsh, J. J., The impact of porosity and crack density on the elasticity, strength and friction of cohesive granular materials: Insights from DEM modelling, *International Journal of Rock Mechanics and Mining Sciences*, **2009**, **46(2)**, pp 250-261.
23. Schöpfer, M. P. J., Childs, C., The orientation and dilatancy of shear bands in a bonded particle model for rock, *International Journal of Rock Mechanics and Mining Sciences*, **2013**, **57**, pp 75-88.
24. Cheung, L. Y. G., O'Sullivan, C., Coop, M. R., Discrete element method simulations of analogue reservoir sandstones, *International Journal of Rock Mechanics and Mining Sciences*, **2013**, **63**, pp 93-103.
25. Wang, Y., Tonon, F., Modeling triaxial test on intact rock using DEM with membrane boundary, *Journal of Engineering Mechanics*, **2009**, **135(9)**, pp. 1029-1037.
26. de Bono, J. P., McDowell, G. R., Wanatowski, D., Discrete element modelling of a flexible membrane for triaxial testing of granular material at high pressures, *Geotechnique Letters*, **2012**, **2(Oct-Dec)**, pp. 199-203.
27. de Bono, J. P., *Discrete element modelling of cemented sand and particle crushing at high pressures*, **2013**, PhD Thesis, University of Nottingham, Nottingham, UK.
28. Collop, A. C., McDowell, G. R., Lee, Y., Use of the Distinct Element Method to Model the deformation Behavior of an Idealized Asphalt Mixture, *International Journal of Pavement Engineering*, **2004**, **5(1)**, pp 1-7.
29. Huang, X., Hanley, K. J., O'Sullivan, C., Kwok, F. C. Y., Effect of sample size on the response of DEM samples with a realistic grading, *Particuology*, **2014**, pp 107-115.
30. Marketos, G., Bolton, M. D., Flat boundaries and their effect on sand testing, *International Journal for Numerical and Analytical Methods in Geomechanics*, **2010**, **34**, pp 821-837.
31. Ergenzinger, C., Seifried, R., Eberhard, P., A discrete element model to describe failure of strong rock in uniaxial compression, *Granular Matter*, **2011**, **13(4)**, pp. 341-364.
32. McDowell, G. R., Amon, A., The application of Weibull statistics to the fracture of soil particles, *Soils and foundations*, **2000**, **40(5)**, pp. 133-141.
33. McDowell, G. R., Statistics of soil particle strength, *Géotechnique*, **2001**, **51(10)**, pp. 897-900.
34. Bolton, M. D., Nakata, Y., Cheng, Y. P., Micro- and macro-mechanical behaviour of DEM crushable materials, *Géotechnique*, **2008**, **58(6)**, pp 471-480.
35. Cuccovillo, T., Coop, M. R., On the mechanics of structured sands, *Géotechnique*, **1999**, **49(6)**, pp. 741-760.
36. Yu, H. S., Tan, S. M., Schnaid, F., A critical state framework for modelling bonded geomaterials, *Geomechanics and Geoengineering*, **2007**, **2(1)**, pp. 61-74.
37. Lo, S. C., Lade, P. V., Wardani, S. P., An experimental study of the mechanics of two weakly cemented soils, *Geotechnical Testing Journal*, **2003**, **26(3)**, pp. 328-341.

Table 1

<b>Sample Properties</b>	
Size: Height x Diameter (mm)	100 x 50
No. of Particles	6759
Friction coefficient	0.5
Normal and shear stiffness (N/m)	$10 \times 10^6$
Density ( $\text{kg/m}^3$ )	2650
Coefficient of uniformity	2.0
Minimum particle diameter (mm)	2.0
Maximum particle diameter (mm)	8.0
Initial voids ratio	0.55
Contact model	Linear springs (default)
Damping coefficient	0.7 (default value)
Bond diameter (mm)	2
Mean bond normal and shear strength ( $\text{N/mm}^2$ )	15.92*
Mean equivalent bond strength in pure tension and pure shear (N)	50*
<b>Membrane Properties</b>	
No. of particles	11979
Friction coefficient	0.0
Normal and shear stiffness (N/m)	$0.6 \times 10^6$
Density	1000
Particle diameter (mm)	1.33